TITLE

DNA Binding Induces a *cis* to *trans* Switch in Cre Recombinase to Enable Intasome Assembly

AUTHORS

Aparna Unnikrishnan[1], Carlos D. Amero[2], Deepak Kumar Yadav[1], Kye Stachowski[1], Devante Potter[1] and Mark P. Foster[1*]

[1]Department of Chemistry and Biochemistry, The Ohio State University, Columbus, Ohio, USA 43210. [2]Laboratorio de Bioquímica y Resonancia Magnética Nuclear, Centro de Investigaciones Químicas, Instituto de Investigación en Ciencias Básicas y Aplicadas, Universidad Autónoma del Estado de Morelos, Avenida Universidad 1001, Colonia Chamilpa, Cuernavaca, Morelos, 62209, Mexico.

*Corresponding Author: Mark P. Foster (email: foster.281@osu.edu; 614-292-1377). Department of Chemistry and Biochemistry, Columbus, OH 43210.

ABSTRACT

Mechanistic understanding of DNA recombination in the Cre-*loxP* system has largely been guided by crystallographic structures of tetrameric synaptic complexes. Those studies have suggested a role for protein conformational dynamics that has not been well characterized at the atomic level. We used solution NMR to discover the link between intrinsic flexibility and enzyme function in Cre recombinase. Remarkably, in the absence of DNA the C-terminal helix αN, implicated in assembly of synaptic complexes and regulation of DNA cleavage activity via *trans* protein-protein interactions, is found to adopt an apparent auto-inhibitory *cis* conformation. Binding to *loxP* DNA dislodges the C-terminus from this *cis* conformation, thereby enabling the *trans* protein-protein interactions required for assembly of recombinogenic Cre intasomes. These findings necessitate a re-examination of the mechanisms by which this widely utilized gene-editing tool selects target sites, avoids spurious DNA cleavage activity, and controls DNA recombination efficiency.

31 **INTRODUCTION**

32 Site specific DNA recombinases represent an attractive option for genome engineering – the
33 insertion or exchange of genes into precise locations in chromosomes[1–4]. The tyrosine
34 recombinase family of phage-derived enzymes (e.g., λ-integrase, Cre and Flp recombinases),
35 which evolved to facilitate viral infection, gene transposition and bacterial pathogenesis, have
36 proven useful for applications that include DNA subcloning without restriction enzymes, and
37 conditional expression of target genes[5–7]. These proteins bind specifically to pairs of inverted
38 short palindromic DNA sequences (*recombinase binding elements*; RBEs) and mediate
39 recombination by assembly of tetrameric *intasomes* (Fig. 1a, b) which perform concerted DNA
40 strand cleavage, exchange and ligation reactions[5,8,9]. Compared to other genome
41 engineering approaches[10,11], site specific DNA recombinases have the advantage that they
42 allow a high degree of specificity, don't require involvement of additional host-encoded
43 factors, and are capable of generating cleanly integrated double-stranded DNA products[3,12–
44 14]. These advantages motivate efforts to understand and manipulate the mechanisms of this
45 family of enzymes.

46 Cre (Causes Recombination) is the best studied member of the tyrosine recombinase
47 family, yet fundamental gaps exist in our understanding of its mechanism of DNA site
48 selection, intasome assembly, and allosteric control of DNA cleavage. The overall
49 mechanism of Cre-mediated DNA recombination has been mapped out via many biochemical
50 and crystallographic studies[5,15–19]. The enzyme catalyzes recombination between a pair of
51 homologous 34 bp *loxP* sites (Fig. 1c) via a highly orchestrated series of events involving
52 recognition and binding of a pair of Cre molecules to its semi-palindromic recognition site
53 containing two RBEs (*loxP* half-sites), “synapsis” of an antiparallel pair of Cre dimers bound
54 to *loxP* to form a stable tetrameric structure, coordinated cleavage of two opposing DNA

55 strands to produce an intermediate with two of the Cre protomers covalently attached to a 3'-
56 phosphate via a tyrosine linkage, followed by strand transfer and re-ligation to form a four-
57 way DNA Holliday junction intermediate[5]. Two-fold asymmetry in the synaptic structures (Fig.
58 1a) is implicated in regulation of DNA strand cleavage activity, and thereby influence the order
59 of strand cleavage and direction by which the Holliday junction is resolved[17,20,21].

60 Although much is known about the overall mechanism of the reactions catalyzed by
61 Cre and related site-specific recombinases, the nature of the conformational changes in the
62 protein and protein-DNA complexes that facilitate the various steps in the pathway remain
63 poorly understood[16,17,19,22–25]. Cre binds its target sequences by forming a C-shaped clamp
64 with a C-terminal catalytic domain (Cre^{Cat}) possessing the namesake tyrosine residue on one
65 side of the DNA, and on the other an N-terminal domain (Cre^{NTD}), connected by an extended
66 8 amino acid linker (Fig. 1). A series of sequential inter-protomer protein-protein interactions
67 across the tetrameric synapse distinguish the structures of the active and inactive protomers.
68 Within the catalytic domain, the tyrosine residue that serves as the nucleophile to catalyze
69 phosphoryl transfer and formation of the covalent intermediate is located on the penultimate
70 helix αM, while the αM-N loop and C-terminal helix αN from each protomer makes a *trans*
71 contact (in a "clockwise" manner as viewed in Fig. 1a) to the neighboring protomer in the
72 tetrameric complex. The β2-3 loop of each protomer abuts its own helix αM, and in the
73 tetramer packs proximally to helix αM of the neighboring protomer, in the opposite direction
74 compared to helix αN. Structural asymmetry in tetrameric structures is localized to these two
75 regions of the protein (Fig. 1a, b). The asymmetry in the C-terminal and inter-protomer
76 interfaces observed in the synaptic complexes of Cre and other tyrosine recombinase family
77 members suggest that the intrinsic dynamic behavior of the enzymes is important in
78 controlling its function, both in mediating tetramer assembly, and for regulating protomer

activity[26–32]. Despite the importance of understanding the basis for conformational differences in Cre, structural insights have been largely limited to crystal structures of isosteric tetrameric synaptic complexes[5,16,17,19].

We have used solution nuclear magnetic resonance (NMR) spectroscopy to explore the link between the intrinsic dynamic behavior of Cre and its function. First, NMR spectra of full-length Cre and of the isolated catalytic domain (Cre^{Cat}) support the premise that the N- and C-terminal domains of Cre are structurally uncoupled. Nuclear spin relaxation experiments reveal flexibility in regions of Cre^{Cat} that are associated with both protein-protein and protein-DNA interactions. Unexpectedly, we found that the region of the protein comprising C-terminal helix αN is not highly dynamic, contrary to the expectation from crystal structures that it would be extended in solution[5,16,17,19]. Instead, NMR chemical shift perturbations and paramagnetic relaxation enhancement (PRE) experiments show the C-terminus of unbound Cre to be located in the DNA binding active site, in an apparent auto-inhibitory conformation. Upon binding to *loxP* DNA, the data show that the C-terminus is displaced, after which it is able to participate in fledgling intermolecular protein-protein interactions with other Cre molecules. These findings shed light on the previous paradoxical reports of *trans* interactions regulating Cre activity[33], and represent a transformative advance in our understanding of the role of protein dynamics in regulating conservative site-specific DNA recombination.

RESULTS

NMR spin relaxation reveals unexpected rigidity in the Cre C-terminal helix αN

To explore the role of protein dynamics in enabling the interconversion of Cre reaction intermediates in solution, we expressed and purified full-length Cre (38.5 kDa, residues 1-343) and a C-terminal fragment encoding the interdomain linker along with the C-terminal domain (23.8 kDa, residues 127-343). This domain, herein termed Cre^{Cat} (Fig. 1b, d) includes all seven active site residues (R173, E176, K201, H289, R292, W315 and Y324), the Cre-DNA binding specificity determinants (R259 and E262) as well as the C-terminal region implicated in *loxP* DNA binding cooperativity and synapsis (Fig. 1a)[17,33–37]. Both full-length Cre and Cre^{Cat} are predominantly monomeric in the absence of DNA, as indicated by their elution times in size exclusion chromatography (Supplementary Fig. 1a). Comparison of 2D ^{1}H-^{15}N TROSY-HSQC correlation spectra of Cre^{Cat} and full-length Cre showed that the well-dispersed signals overlay well (Supplementary Fig. 1b). This indicates that Cre^{Cat} folds independently in solution and that the N-terminal domain of Cre does not interact with the catalytic domain in solution, thereby justifying structural and dynamics studies of the isolated domain.

For backbone resonance assignments of Cre^{Cat} we expressed, purified the [U-^{15}N] and [U-^{15}N,^{13}C] labeled protein and recorded HSQC- and TROSY-based double- and triple-resonance NMR spectra. Homogeneity and integrity of protein constructs were verified by SDS-PAGE and mass spectrometry (data not shown). We obtained backbone resonance assignments for 195 of 214 non-proline amides (> 91%) (Fig. 1d, Supplementary Fig. 2 and 3). Unassigned amide resonances include the two N-terminal residues (A127 and G128), and a few residues in the loop regions of Cre^{Cat}, due to line broadening from intermediate conformational exchange.

123 To probe the fast timescale backbone dynamics in Cre^{Cat}, we measured ^{15}N NMR (R_1,
124 R_2) and $\{^1H\}$-^{15}N heteronuclear NOE (HetNOE) relaxation data (Fig. 2). The data show that
125 Cre^{Cat} backbone amides largely exhibits uniform relaxation rates, with an overall rotational
126 correlation time (τ_C) of 13.2 ± 0.9 ns, computed from the trimmed-mean R_2/R_1 ratios[38].
127 Distinctly lower R_2/R_1 ratios and decreased $\{^1H\}$-^{15}N hetNOE values indicating fast (ps-ns)
128 internal motions, were observed for the linker residues through A134 preceding αF, the β2-3
129 loop, αJ-K loop, αM-N loop and a few residues after the C-terminal helix αN. The β2-3 loop
130 forms inter-protomer contacts in Cre-DNA synaptic tetramers and adopts distinct
131 conformations between the catalytically "active" and "inactive" forms of Cre (Fig. 1a, b)[5]. The
132 data show the αJ-K loop to be flexible in free Cre^{Cat} though it does not differ structurally
133 between the two Cre isomers, consistent with a role in DNA binding, not in regulating
134 recombination[5]. Surprisingly, although residues bracketing the C-terminal helix αN exhibit
135 evidence of fast internal motions, the relaxation rates for the helix αN (A334- L339) are close
136 to the average values, indicating that it tumbles with the catalytic core of the protein. This
137 suggests that instead of being extended in solution as might be expected from the *trans*
138 conformations observed in tetrameric crystal structures, αN might adopt a distinct
139 conformation in the free protein.

140

141 **Truncation of C-terminal helix αN results in widespread CSPs in the core of Cre^{Cat}**

142 In tetrameric DNA-bound crystal structures of Cre, the C-terminal helix αN of each protomer
143 packs in *trans* in a cyclic (non-reciprocal) manner into a surface cavity on a neighboring
144 protomer composed of residues from αF, αG, αH, β2-3 loop, αI, αK and αL regions (Fig. 1a).
145 Since Cre is monomeric in the absence of DNA, the Van Duyne group had previously used
146 crosslinking experiments to test the hypothesis that in free Cre the C-terminal region folds

147 back to dock over its own *trans* cavity in *cis*; those experiments failed to detect intramolecular
148 crosslinks[39]. Nevertheless, the ^{15}N relaxation data (Fig. 2) would be consistent with a *cis*
149 docking model in which rotational diffusion of αN is coincident with overall tumbling of the
150 protein.

151 To test whether the C-terminal region of Cre^{Cat} might be docked in *cis*, instead of being
152 extended for *trans* docking, we examined the effect of deleting the C-terminal residues on the
153 NMR spectra. We constructed a C-terminal deletion lacking thirteen C-terminal residues
154 including helix αN: Cre^{Cat}ΔC (residues 127- 330), obtained backbone resonance assignments
155 from triple resonance NMR data, and compared the ^{1}H-^{15}N TROSY-HSQC spectra of WT
156 Cre^{Cat} and Cre^{Cat}ΔC (Fig. 3a, Supplementary Fig. 4). Large chemical shift perturbations
157 (CSPs) were observed for residues in the interdomain linker region (Q133- A136), helices
158 αH, αK, αM and the αJ-K loop (Fig. 3a). Each of the regions in the protein core that show
159 large CSPs is in excess of 20 Å from the center of helix αN in the synaptic structures. These
160 findings are consistent with a *cis* docking arrangement of the C-terminus, and with the
161 restricted internal motions inferred from ^{15}N relaxation studies.

162 Remarkably, when the CSPs for Cre^{Cat}ΔC are mapped to the crystal structure of the
163 protein (Fig. 3b), the CSPs do not map to the synaptic *trans* docking surface of Cre. The
164 region of the interdomain linker that shows large CSPs (Q133- A136) is adjacent to the DNA
165 binding surface and was found to be largely rigid on the ps-ns timescale (Fig. 2). Helix αH
166 contains active site residues R173 and E176, αJ-K loop and helix αK contain the active site
167 residues H289 and R292, while helix αM contains the active site residue Y324.

168 These CSPs show that deletion of the C-terminal region alters the environment of
169 residues surrounding the active site of Cre and part of its DNA binding surface. To ensure
170 that the CSPs observed in these experiments are not an artifact of working with the catalytic

171 domain Cre^{Cat}, we compared spectra between full-length Cre and the same C-terminal
172 deletion: CreΔC (residues 1-330). An overlay of ^{1}H-^{15}N TROSY-HSQC spectrum of full-length
173 Cre on that of CreΔC showed the same CSPs for residues from the catalytic domain, and
174 minimal perturbation of signals attributed to Cre^{NTD} (Supplementary Fig. 5). Although CSPs
175 can be due to either direct or indirect interactions[40,41], the Cre^{Cat}ΔC CSP data suggest that
176 the C-terminal residues in Cre^{Cat} pack in *cis* over the active site and DNA binding surface of
177 Cre^{Cat}, not over the *trans* docking surface.

178

179 **PRE-NMR data support *cis* docking of C-terminal helix αN of Cre**

180 To clarify whether the CSPs in the core of Cre^{Cat} domain were induced by direct interactions
181 or via indirect allosteric effects, we attached a nitroxide spin probe at the extreme C-terminus
182 of Cre^{Cat} and performed paramagnetic relaxation enhancement (PRE)-NMR experiments[42–
183 44]. We constructed a variant of Cre^{Cat} (C155A/C240A/D343C) that enabled attachment of the
184 spin probe to the C-terminal cysteine residue and used ^{1}H-^{15}N TROSY-HSQC spectra to
185 verify that the mutations did not significantly perturb the structure of the protein (data not
186 shown). The single cysteine mutant was then conjugated with a S-(1-oxyl-2,2,5,5-tetramethyl-
187 2,5-dihydro-1H-pyrrol-3-yl) methyl methanesulfonothioate (MTSL) paramagnetic spin probe.
188 Near 100% tagging efficiency was verified using MALDI mass spectrometry (data not shown).
189 ^{1}H-^{15}N TROSY-HSQC spectra of the MTSL tagged-protein under oxidized (paramagnetic)
190 and reduced (diamagnetic) conditions were obtained and a comparison of the peak intensities
191 was used to determine per-residue PRE effects in free Cre^{Cat}. In such a PRE-NMR
192 experiment, the lone-pair electron on a paramagnetic spin probe is expected to induce
193 distance-dependent line broadening for protons up to 25 Å away[45].

194 A strong correspondence between the C-terminus-linked PRE effects and previously
195 observed CSPs provide evidence for *cis* packing of the C-terminus over the active site and
196 DNA binding surface of Cre. In addition to residues sequentially neighboring C343, we
197 observed strong PRE effects from the C-terminal C343-MTSL spin probe to a part of the
198 interdomain linker (E129- A136), helix αH (R173- A178), helix αJ (S257- I264), αJ-K loop
199 (L284- R292) and helix αM (G314- Y324) (Fig. 4a, Supplementary Fig. 6). To interpret the
200 PRE effects in a structural context, we built a model of the MTSL tagged-protein using
201 PyMOL[46] with PDB ID 2HOI, chain B as the template, manually added the two missing C-
202 terminal residues (G342, C343), D343 substituted with cysteine, and attaching an MTSL
203 moiety (coordinates from PDB ID 2XIU)[47] to the C343 sidechain, and mapped the PRE data
204 onto this Cre^{Cat} structural model (Fig. 4c: left). Each of the regions showing strong PRE effects
205 in free Cre^{Cat} are at distances in excess of 25 Å as measured from the C343-MTSL-oxygen
206 to backbone amide nitrogen atoms: further than ~ 42 Å, ~ 47 Å, ~ 51 Å, ~ 42 Å, and ~ 37 Å,
207 respectively (Supplementary Fig. 6a).

208 To rule out the possibility that the observed PRE effects were due to intermolecular
209 interactions, we performed an intermolecular PRE experiment by recording ^{1}H-^{15}N TROSY-
210 HSQC spectra of a 1:1 mixture of [U-^{15}N]-Cre^{Cat} (non-tagged) with MTSL tagged- unlabeled
211 Cre^{Cat} C155A/C240A/D343C, under paramagnetic and diamagnetic conditions. Because the
212 ^{15}N labels and MTSL tags are on different molecules any PRE effects must arise from
213 intermolecular interactions (Supplementary Fig. 7a)[48]. Only a few sparse residues located in
214 the *trans* docking surface of Cre showed intermolecular PRE effects, suggestive of very weak
215 transient intermolecular interaction (Supplementary Fig. 7b, c). Thus, the strong
216 intramolecular PRE effects in the ^{1}H-^{15}N TROSY-HSQC amide spectrum of free Cre^{Cat}

217 strongly support a model in which the C-terminal region makes a *cis* interaction with its own
218 DNA binding surface (Fig. 4c: left and right).

219

220 **PRE-restraints yield a *cis* docked model of the C-terminus of Cre, consistent with CSPs**

221 To determine whether the covalent structure of Cre^{Cat} would allow *cis* docking of helix αN region
222 without distorting other structural elements, we performed structure refinement using PRE-
223 derived distances as restraints. Analysis of the free Cre^{Cat} PRE I_{ox}/I_{red} values and ^{15}N R_2 relaxation
224 rates yielded 124 restraints (Supplementary Table 1). To account for a distribution of spin probe
225 positions, lower bounds were set to 5 Å below calculated distances while the upper bounds were
226 set to 10 Å higher than the calculated distances. ROSETTA energy minimization was performed
227 using upper and lower distance bounds, assuming a flexible C-terminus, β2-3 loop and αJ-K loop
228 regions; crystallographically observed secondary structure elements were enforced. Members of
229 the PRE-derived Cre^{Cat} ensemble (Fig. 5a) adopt stereochemically robust *cis* docked C-terminal
230 conformations that differ significantly from the conformation observed in synaptic complexes (Fig.
231 5b). These structures are consistent with CSP data, even though those were not used during
232 refinement (Fig. 5c). Difference Cα-Cα contact map between the top ten conformers and the
233 synaptic crystal structure (PDB ID 2HOI, chain A) show that the average changes in C-terminal
234 inter-residue distances when *cis* docked, ranged in values as large as 25 Å (Fig. 5d).

235

236 **DNA binding perturbs the C-terminal region in Cre^{Cat}**

237 Coincidence of the DNA binding site and *cis* docking surface of the Cre^{Cat} C-terminal region
238 led us to examine the effects of binding to a *loxP* DNA half-site substrate (Fig. 1c), on the
239 protein C-terminus. The ^{1}H-^{15}N TROSY-HSQC spectrum of the Cre^{Cat}-DNA half-site complex
240 showed CSPs in residues corresponding to the Cre-DNA interaction surface, comprising of

241 structural elements involved in DNA binding and the active site regions. Moreover, large
242 CSPs (and broadening of resonances) were also observed in the C-terminal residues E331-
243 D343, including helix αN (Fig. 6a, b). The CSPs mapped on the crystal structure (Fig. 6c)
244 show that *loxP* DNA half-site binds to Cre^{Cat} in the manner predicted from available tetrameric
245 structure models, but DNA binding also induces a change in the environment of the C-terminal
246 residues, resulting in the observed CSPs.

247

248 **PRE-NMR data reveal a DNA binding-induced conformational change in the Cre C-**
249 **terminus**

250 Like for the free protein, we used PRE-NMR to determine the conformational space
251 populated by the C-terminus of Cre upon binding to *loxP* DNA half-site. PRE effects were
252 measured using MTSL tagged-Cre^{Cat} C155A/C240A/D343C bound to the *loxP* half-site
253 hairpin DNA. PRE effects were remarkably different in the DNA complexes in comparison to
254 free Cre^{Cat} (Fig. 4b, Supplementary Fig. 8). Low I_{ox}/I_{red} ratios were observed for helix αF
255 (E138- M149), helix αG (G165- E176), β2 and β2-3 loop (G191- I195, G198 and V204), β3-
256 αI region (A212- R223), and helices αK- αL region (A291- G314). These regions together
257 form the *trans* docking cavity that accommodates the C-terminus of neighboring Cre
258 protomers in synaptic complexes (Fig. 1a, 4d: left and right). This change in PRE pattern (Fig.
259 4a versus 4b) clearly identifies a DNA-induced conformational change that involves
260 displacing the C-terminus from the DNA binding surface, to enable new protein-protein
261 interactions; however, they do not establish whether those new interactions occur in *cis*
262 (intramolecular), or in *trans* (intermolecular).

263 Intermolecular PRE-NMR studies with mixed isotopic labeling were then used to clarify
264 whether the PRE effects observed in the presence of DNA arise from intra or intermolecular

265 interactions. We mixed DNA-bound non-tagged [U-^{15}N]-Cre^{Cat} and MTSL-tagged unlabeled
266 Cre^{Cat} C155A/C240A/D343C at a 1:1 molar ratio, to study possible intermolecular interactions
267 in Cre^{Cat} bound to DNA. Because these mixed samples have the potential to interact in four
268 different relative orientations (Supplementary Fig. 9a), only one of which would generate
269 measurable PRE effects (i.e., MTSL tagged- unlabeled Cre^{Cat} C155A/C240A/D343C with C-
270 terminus docking onto a [U-^{15}N]-Cre^{Cat}), the experiment would be predicted to yield weaker
271 PRE effects in comparison to the experiments with uniformly labeled and MTSL tagged-
272 Cre^{Cat}-DNA complex (Fig. 4b); although observation of such effects in the same regions of
273 the protein would support *trans* interactions. Despite the resonances being broader and data
274 quality being generally lower, we indeed observed strong PRE effects consistent with docking
275 of DNA-bound Cre C-terminal region over the *trans* docking surface (Supplementary Fig. 9b,
276 c); these effects *must* arise from intermolecular interactions because of the labeling pattern
277 used. Yet, a comparison to the similarly strong PRE effects in uniformly tagged and labelled
278 Cre^{Cat}-DNA complex studies (Supplementary Fig. 9c versus Fig. 4b) illustrates the possibility
279 of a population of DNA-bound Cre C-terminus docking in *cis* over its own *trans* docking cavity,
280 while another population extends out to dock in *trans* into the same cavity on another DNA-
281 bound Cre molecule.

282

283 **DISCUSSION**

284 Cre recombinase has emerged as an important tool in molecular and cellular biology and has
285 several features that make it an attractive reagent for gene editing[7,49,50]. Reaching that
286 potential requires thorough characterization of its mechanism for DNA site selection, and
287 control of its DNA cleavage and recombination activity. High-resolution structural studies of
288 Cre, largely limited to crystal structures of DNA bound tetrameric synaptic complexes, have

289 suggested a role for conformational plasticity in facilitating the steps within the reaction
290 mechanism. We set out to characterize the solution behavior of Cre in its free and DNA bound
291 states in order to understand the link between protein dynamics and regulation of Cre
292 assembly and activity. While solution NMR studies yielded some results consistent with
293 previous understanding of this prototypical member of the tyrosine recombinase family, other
294 surprising results call for a revised view of the reaction mechanism.

295 Solution NMR data showed Cre^{Cat} to be independent of Cre^{NTD}. The well-dispersed
296 signals in the ^{1}H-^{15}N TROSY-HSQC NMR spectrum of Cre^{Cat} are nearly superimposable on
297 that of full-length Cre, except for the signals attributable to N-terminal domain Cre^{NTD}
298 (Supplementary Fig. 1b). The domains' structural independence could imply variability in
299 inter-domain orientations that would be expected to prevent formation of suitable crystal
300 lattices for x-ray diffraction. It however facilitated detailed NMR studies with the Cre^{Cat} domain,
301 wherein reside the active site residues and sequence specificity determinants, focused on
302 testing the role of protein dynamics in regulation of Cre function[33–36].

303 Our findings of the protein dynamics in specific regions within Cre^{Cat} revealed unique
304 spectral signatures linked to their functional roles. Underlying flexibility in Cre^{Cat} revealed by
305 nuclear spin relaxation measurements (^{15}N R_1, R_2 and $\{^{1}H\}$-^{15}N HetNOE), were consistent
306 with the monomeric 217-residue protein construct (τ_C, 13.2 ns). A portion of the linker, the
307 β2-3 loop, the αJ-K loop and the αM-N loop each exhibit higher R_1, lower R_2, and reduced
308 HetNOE values, indicative of fast internal motions. Within the Cre_4-*loxP*$_2$ tetrameric synaptic
309 complexes, conformational differences in the β2-3 loop and the C-terminal regions (including
310 helix αN) that form structural bridges that link adjacent protomers, and in helix αM bearing
311 the catalytic tyrosine, distinguish the catalytically "active" and "inactive" Cre protomers[5,16,22].
312 Flexibility of the β2-3 loop observed in free Cre^{Cat} could be expected to prevent stabilization

313 of the active site geometry in uncoordinated Cre protomers. The alternating conformations of
314 the loop in tetrameric synaptic complexes indicates that this flexibility will be still retained,
315 thereby enabling its regulatory role over adjacent active site structures. The protein dynamics
316 observed in the αJ-K loop in the free protein may serve to facilitate DNA binding and could
317 thereafter be predicted to undergo quenching since this region does not show structural
318 plasticity between the various Cre reaction intermediates. The surprise within the protein
319 dynamics analysis lies in the observation that while residues flanking C-terminal helix αN
320 exhibit flexibility on the ps-ns timescale, αN itself does not, and instead exhibits relaxation
321 rates consistent with overall tumbling of the protein, counter to the expectation that the Cre
322 C-terminus would flexibly adopt a range of extended conformations to facilitate capturing an
323 adjacent protomer via *trans* docking contacts.

324 An unexpected C-terminal *cis* docking interaction in the proximity of the free Cre active
325 site was revealed from our highly correlated CSP and PRE-NMR experiments. Given the
326 known *trans* docking site, and prior incongruities regarding *cis* or *trans* cleavage by Cre and
327 other recombinases[51], a logical presumption was that in free Cre, helix αN might dock in *cis*
328 in the same site it occupies when assembled in *trans* in synaptic complexes; indeed, such a
329 premise was previously tested experimentally using disulfide crosslinking strategies[39]. Were
330 that the case, one would predict that deletion of helix αN would result in CSPs for residues
331 flanking that *trans* docking surface cavity. Instead, we observed the largest CSPs for residues
332 on the other side of the protein – namely, the DNA binding and active site surfaces (Fig. 3).
333 Since CSPs can arise from both proximity and induced conformational changes, we employed
334 distance-dependent effects in PRE-NMR experiments to conclusively demonstrate the
335 proximity of the protein C-terminus to the active site and DNA binding regions (Fig. 4a).
336 Consistent with size exclusion chromatography (Supplementary Fig. 1a), NMR relaxation

337 (Fig. 2) and previous sedimentation velocity experiments[17] that show unbound Cre to be
338 monomeric in solution, the absence of strong intermolecular PREs (Supplementary Fig. 7)
339 indicates that docking of the C-terminus of free Cre onto the DNA binding surface indeed
340 occurs *intra*-molecularly, in *cis*. *Cis*-docked models generated using distance bounds derived
341 from the PRE data satisfy the restraints, covalent structure, and are in excellent agreement
342 with the CSPs obtained upon deletion of the C-terminal region (Fig. 5). A comparison between
343 the free Cre^{Cat} ensemble model and the Cre^{Cat} structure from crystallographic DNA bound
344 synaptic complex protomers shows changes in inter-residue contacts as large as 20- 25 Å
345 (Fig. 5d). Thus, these data provide strong evidence that in the absence of DNA the C-terminal
346 residues dock in *cis* over the DNA binding and active site surfaces, in an apparent auto-
347 inhibitory state.

348 A Cre structure in which the C terminus is docked in *cis* over the active site would
349 seem incompatible with a DNA-bound state – so, how is this conundrum resolved? PRE-NMR
350 data on the Cre^{Cat}-DNA complex show that the C-terminus of Cre^{Cat} is displaced from the *cis*
351 docking surface when DNA binds there, since PRE effects are instead observed at the *trans*
352 docking cavity (Fig. 4b). This *loxP* binding-induced pattern of PREs at the *trans* docking site
353 clearly indicates relocation of C-terminal helix αN, but does not clarify whether docking occurs
354 in *cis*, or in *trans* to a nearby Cre molecule. The use of a DNA *loxP* half-site substrate would
355 be expected to prevent assembly of pre-synaptic complexes with two Cre molecules bound
356 to DNA; however, PRE effects can be observed even when interactions are transient[52].
357 Although partially attenuated, intermolecular PRE effects were indeed observed at the same
358 *trans* docking cavity in experiments where the NMR signals from DNA-bound Cre^{Cat} arise
359 from protein molecules not tagged with MTSL (Supplementary Fig. 9). This attenuation could
360 result from the fact that only one-fourth of protein-protein contacts within DNA-bound

361 complexes can produce *intermolecular* PRE effects (i.e., when C-terminus from MTSL-tagged
362 un-labeled Cre^{Cat} docks in *trans* over non-tagged [U-^{15}N]-Cre^{Cat} when bound to DNA;
363 Supplementary Fig. 9a), or may indicate that in the presence of DNA, *intramolecular cis*
364 docking over the protomer's own *trans* docking cavity is also possible. However, molecular
365 modeling calculations starting from the DNA-bound crystal structure (data not shown)
366 indicated that the C-terminal helix αN region could not pack over its own *trans* docking cavity
367 without significant conformational strain, involving additional remodeling that would be
368 inconsistent with the NMR CSP data (Fig. 5). We conclude that in the absence of DNA, the
369 C-terminal residues spanning helix αN occupy the DNA binding surface of Cre, and that
370 binding to DNA produces a large conformational change that enables productive *trans*
371 protein-protein interactions with adjacent Cre molecules.

372 The rigidity and apparent auto-inhibitory conformation observed in C-terminal residues
373 in free Cre could be expected to disfavor oligomerization of the protein prior to *loxP* DNA
374 binding and play a role in selectively inhibiting spurious uncoordinated DNA cleavage and
375 recombination activity. Although it is unclear whether the *cis* docking conformation of C-
376 terminal region in free Cre serves additional roles, for example by obstructing inadvertent
377 binding to non-cognate DNA substrates, our data suggests that the conformational
378 rearrangements following the displacement of *cis* docking C-terminal upon *loxP* DNA half-site
379 binding, comprise the mechanistic step that could trigger Cre protomer stepwise assembly on
380 *loxP* through protein-protein interactions via the now exposed C-terminal residues.

381 These studies expand our understanding of the regulatory role played by C-terminal
382 residues in Cre [5,16,17]. DNA-binding associated conformational changes mediated by C-
383 terminal regions of Cre and related recombinases have been implicated in catalytic activation
384 and initiation of oligomerization[2,5,28]. However, the structural basis for Cre to undergo

385 stepwise assembly on the DNA recognition sites have remained poorly understood due to
386 lack of structural information on pre-synaptic reaction intermediates. The features of Cre and
387 Cre-*loxP* complexes presented here provide insight into both the unliganded state of Cre, as
388 well as the mechanism of initiation of protein-protein interactions that lead to stepwise
389 assembly of recombinogenic intasomes. Knowledge gaps remain, including understanding of
390 precise structural rearrangements that accompany the *cis* to *trans* switch in pre-synaptic Cre
391 recombinase. Nevertheless, these investigations provide a new NMR perspective on Cre
392 recombinase and represent a transformative step towards understanding the structure,
393 function and mechanism of this important and widely used gene editing tool.
394

395

396 **METHODS**

397 **Protein expression, purification, and site-directed mutagenesis**

398 The deletion construct containing the catalytic domain and the interdomain linker (Cre^{Cat},
399 residues 127- 343) was prepared using QuikChange Site-Directed Mutagenesis Kit (Agilent)
400 from a pET21A vector (Novagen) encoding WT Cre Recombinase (provided by Dr. Gregory
401 Van Duyne, U. Penn). Further truncation and point mutants of Cre^{Cat} construct were prepared
402 using the Q5 Site-Directed Mutagenesis Kit (NEB). Protein expression from *E. coli* BL21(DE3)
403 cells was carried out by growing freshly transformed cells (using Ampicillin antibiotic, 100
404 mg/L) in LB media (natural abundance Cre) or M9 minimal medium (isotopically labeled [U-
405 ^{15}N] and [U-^{13}C,^{15}N] Cre) supplemented with 1 g/L [^{15}N]-ammonium chloride (Cambridge
406 Isotopes) as the sole nitrogen source or 2 g/L [^{13}C]-glucose (Cambridge Isotopes) as the sole
407 carbon source in addition to [^{15}N]-ammonium chloride. The cells were grown (shaking at 220
408 rpm, 37 °C) to an OD_{600} of 0.6- 0.8 and induced with 0.75 mM isopropyl β-D-1-

409 thiogalactopyranoside (Gold Biotechnology) for 12 h. After harvesting the cells (4000 g, 15
410 min, 4 °C) and sonication, the Cre constructs in 40 mM tris, 100 mM NaCl, pH 7.0 buffer
411 containing 1 protease inhibitor cocktail tablet (Roche), were purified using 5 ml SPFF cation
412 exchange column (GE Healthcare) with a 100 ml gradient of 0.1 to 1 M NaCl. The protein
413 fractions (eluted at ~ 0.4 M NaCl) were combined and diluted four times with low salt buffer
414 40 mM tris, 100 mM NaCl pH 7.0 and further purified on a 5 ml Heparin affinity column (GE
415 Healthcare) with a 100 ml gradient of 0.1 to 1.5 M NaCl. Protein fractions (eluted at ~ 1 M
416 NaCl) were then purified using a HiLoad 16/60 Superdex 75 (GE Healthcare) column (SEC)
417 in 40 mM tris, 500 mM NaCl pH 7.0 buffer. Purified protein concentrations were determined
418 using UV-Vis spectroscopy (ε for Cre^{Cat} = 23,950 M^{-1} cm^{-1} at 280 nm). Typical yields obtained
419 were ~20-25 mgs protein per L of culture.

420

421 **Cre^{Cat}-DNA complex NMR sample preparation**

422 *loxP* half-site hairpin was formed from single-stranded DNA oligos (IDT) containing
423 recombinase binding elements along with additional GC bps at ends, symmetrized spacer
424 bps and a GAA hairpin[53]:

425 5'-GCATAACTTCGTATAGCATATGCGAAGCATATGCTATACGAAGTTATGC-3'.

426 The lyophilized DNA oligo was resuspended in H_2O and heated at 95 °C for 15 mins and
427 immediately cooling on ice. To avoid precipitation, Cre^{Cat} and *loxP* DNA hairpin at low
428 concentrations (< 50 μM) in high salt buffer (10 mM Tris, > 500 mM NaCl, pH 7.0) were mixed
429 by stepwise titration of the protein into DNA. The solution was then dialyzed into low salt NMR
430 buffer (10 mM tris, 15 mM NaCl, 0.02% NaN_3, pH 7.0) at 4 °C. The protein-DNA complex
431 sample was then concentrated using 500 μL, 1 kDa centrifugal filters (VWR).

432

433 **NMR data collection**

434 Purified [U-^{15}N]- or [U-^{15}N,^{13}C]- Cre^{Cat} samples were concentrated to 0.5- 1.0 mM after dialysis
435 into buffer containing 10 mM Tris, 100 mM NaCl, 0.02 % NaN_3, pH 7.0. When required, the
436 samples were exchanged into 10 mM d_{11}-Tris (Sigma), 100 mM NaCl, 0.02 % NaN_3, pH 7.0
437 buffer, using Sephadex PD10 columns (GE Healthcare). 5-10 % (v/v) D_2O (99 %) and 0.66
438 mM DSS were added to the NMR samples. NMR data were recorded on Bruker Avance III
439 HD spectrometers operating at 850, 800 or 600 MHz equipped with a 5 mm triple resonance
440 cryoprobes and z axis gradients, at 25 °C. Data were processed with NMRPipe[54] or NMRFx[55]
441 and visualized using NMRView[56]. Typical ^{1}H-^{15}N TROSY-HSQC 2D correlation spectra were
442 recorded using 16- 24 scans and 2048 x 128 data points.

443

444 **NMR chemical shift assignment and perturbation mapping**

445 For backbone chemical shift assignments, TROSY triple-resonance spectra HNCO, HNCA,
446 HN(CO)CA, HN(CA)CO, and non-TROSY CBCA(CO)NH and HA(CO)NH were recorded on
447 purified [U-^{13}C,^{15}N] Cre^{Cat} sample. Backbone assignment was achieved using NMRView
448 aided by PINE[57] and CARA[58].

449 CSPs were calculated from differences in peak positions using:

450 $$\Delta\delta_{NH} = \sqrt{\Delta\delta_H{}^2 + \frac{(\Delta\delta_N)^2}{25}}$$

451 where $\Delta\delta_H$ is the chemical shift difference in the ^{1}H dimension and $\Delta\delta_N$ is the chemical shift
452 change in the ^{15}N dimension. Corrected standard deviations were determined by calculating

453 the SD of CSPs of all assigned residues, removing CSP data with > 3 SD and recalculating
454 the SD.

455

456 **^{15}N relaxation measurements**

457 Backbone amide relaxation measurements were performed at 800 MHz proton Larmor
458 frequency using [U-^{15}N] Cre^{Cat} at a concentration of 800 μM in 10 mM Tris, 100 mM NaCl,
459 0.02 % NaN_3, pH 7.0 buffer (5 % D_20 v/v). TROSY versions of R_1 and R_2 experiment data
460 were acquired using recycle delay of 2 seconds between experiments, and the following
461 relaxation delays for R_1: 0, 560, 1120 and 1680 ms with repeats and R_2: 2, 24.2, 48.2, and
462 72.2 ms. The R_1 and R_2 values were obtained by fitting the intensity of peaks to exponential
463 decay function and errors were determined by relaxation curve fitting. 80-90 % of the amides
464 were analyzed, after excluding those with significant resonance overlap. {^{1}H}-^{15}N HetNOE
465 values were obtained by recording spectra with and without a ^{1}H pre-saturation period (8 s),
466 in which ^{1}H signals were saturated using a train of 90° pulses, applied before the start of
467 experiment. Non-overlapping assigned peaks were analyzed and the intensity ratio were
468 determined using the HetNOE analysis tool within NMRViewJ; uncertainties were obtained
469 from standard deviation of noise in the spectra.

470

471 **Paramagnetic Relaxation Enhancement (PRE) - NMR**

472 We constructed a single-cysteine Cre^{Cat} variant C155A/C240A/D343C to avoid unintended
473 paramagnetic tagging of the native cysteines and thereby enable probing just the C-terminus.
474 S-(1-oxyl-2,2,5,5-tetramethyl- 2,5-dihydro-1H-pyrrol-3-yl) methyl methanesulfonothioate
475 (MTSL) tagging of Cre^{Cat} C155A/C240A/D343C was achieved by following a published

476 protocol[59]. Briefly, a 200 mM MTSL (Toronto Research Chemicals) stock was made by adding
477 189 µL of acetonitrile to 10 mg of MTSL (stored at -20 °C, protected from light). DTT was
478 added to purified protein in high salt conditions (10 mM Tris, 500 mM NaCl, 5 mM DTT, pH
479 7.0) to reduce possible disulfide bonds. The reducing agent was then removed by rapid buffer
480 exchange into 10 mM Tris, 500 mM NaCl, pH 7.0 buffer using a PD10 desalting column (GE
481 Healthcare). The sample was collected into exchange buffer containing ten-fold molar excess
482 of MTSL and stirred at room temperature overnight. Excess MTSL was removed after reaction
483 by buffer exchange with a second PD10 column, followed by dialysis (MWCO 3 kDa) into
484 NMR buffer. Near 100 % MTSL tagging of the protein was verified using MALDI MS
485 measurements as indicated by an increase in mass by 186 Da (weight of attached probe).
486 Final sample concentrations ranged between 100-200 µM at a volume of ~ 500 µL.

487 For PRE-NMR measurements, ^{1}H-^{15}N TROSY-HSQC spectra were recorded on the same
488 MTSL tagged-Cre^{Cat} C155A/C240A/D343C sample before (paramagnetic) and after
489 (diamagnetic) reduction of the spin probe by treatment with five-fold molar excess of sodium
490 ascorbate (250 mM stock used for minimal sample dilution) for three hours at room
491 temperature. Peak intensities were measured and normalized using intensities of residues
492 (D153, E222, V230) > 45 Å away from C-terminus in PDB ID 2HOI, chain B. For MTSL
493 probes, I_{ox}/I_{red} ratios between 0 and 1 indicate that the distance of probe to proton is within
494 13- 25 Å. Uncertainties in I_{ox}/I_{red} values were propagated from signal-to-noise ratio of each
495 resonance in the two spectra using:

496 $$\sigma I_{ox}/I_{red} = I_{ox}/I_{red}\sqrt{\left(\frac{\sigma I_{ox}}{I_{ox}}\right)^2 + \left(\frac{\sigma I_{red}}{I_{red}}\right)^2}$$

497 where $\sigma I_{ox}/I_{red}$ is the calculated error in I_{ox}/I_{red} ratio, σI_{ox} is the standard deviation of the noise
498 in the MTSL oxidized spectrum, and σI_{red} is the standard deviation in the reduced spectrum.

499 For the intermolecular PRE studies, [U-^{15}N]-Cre^{Cat} (non-MTSL-tagged) was mixed with MTSL
500 tagged-natural abundance Cre^{Cat} C155A/C240A/D343C, at a 1:1 molar ratio in NMR buffer
501 (10 mM Tris, 100 mM NaCl, pH 7.0) at 25 °C. For similar studies with the protein-DNA
502 complex, the complex samples with/without MTSL tags were prepared separately and mixed
503 at a molar ratio of 1:1.

504

505 **PRE-restrained modeling using ROSETTA**

506 PRE derived-distance constraints for use in structural modeling were generated using the
507 approach of Battiste and Wagner[42]. Briefly, per residue R_2^{sp} values (paramagnetic relaxation
508 rate due to the spin tag) were obtained from:

509 $$I_{ox}/I_{red} = \frac{R_2 e^{-R_2^{sp} t}}{R_2 + R_2^{sp}}$$

510 where R_2 is the transverse relaxation rate of each amide and t is the acquisition time in the
511 proton dimension. R_2^{sp} values were then used to obtain the approximate distance, r (Å)
512 between the spin tag to the amide proton of each residue:

513 $$r = \left[\frac{K}{R_2^{sp}}\left(4\tau_C + \frac{3\tau_C}{1 + \omega_h^2 \tau_c^2}\right)\right]^{\frac{1}{6}}$$

514 where τ_C (s) is per-residue correlation time of amide protons determined from R_2/R_1 relaxation
515 ratios, ω_h (Hz) is the Larmor frequency of each amide proton, and K is a constant (1.23 x 10^{-}
516 ^{32} cm^6 sec^{-2}) that encapsulates the spin properties of the MTSL tag[42].

517 Distance restraints were used in a bounded form (typical for NOE constraints). Due to the
518 relative imprecision of this method of constraint distance calculation[44,60], residues with an
519 I_{ox}/I_{red} value less than 0.8 were assigned a lower bound of calculated *r* - 5 Å and an upper

520 bound was set to r + 10 Å. Residues with an I_{ox}/I_{red} value greater than 0.8 were assigned a
521 lower bound of 20 Å and no upper bound. Constraints for 124 residues in Cre^{Cat} were obtained
522 wherein data (I_{ox}, I_{red}, R_2, ω_h, and τ_C) for each amide proton was available.

523 ROSETTA energy minimization was performed using the relax application[61–65]. Chain
524 A of PDB ID 2HOI (residues 127- 341, and G342 and D343C modeled) was used as the input
525 structure with the D343C mutation. A move map file retained secondary structure of Cre^{Cat}
526 along with the following impositions: the β2-3 and αJ-K loops and interdomain linker residues
527 (A127-A134) were allowed to have backbone φ, ψ, and sidechain χ_1 torsional freedom based
528 on flexibility observed via ^{15}N R_2/R_1 data. C-terminal E331- C343 were also allowed to sample
529 backbone and χ_1 angles allowing movement of helix αN through space. Other residues were
530 only allowed to undergo sidechain minimization. Constraints were used to generate 100 initial
531 structures subsequently scored using the ref2015_cst weights function[66]. The ten structures
532 with the lowest *atom_pair_constraint* energy were selected as the input structures for a
533 second round of minimization wherein ten structures were generated for each input structure.
534 The resulting 100 structures constitute the PRE-NMR constrained ensemble model of free
535 Cre^{Cat}. Coarse grained contact maps were generated using MATLAB by calculating backbone
536 inter-residue Cα-Cα distances from PDB files (2HOI, chain A residues 127- 341 and G342
537 and D343C modeled, and top ten lowest energy members of free Cre^{Cat} PRE-derived
538 ensemble). Absolute values of change in inter-residue distances between the contact maps
539 were determined by subtracting one distance matrix from the other.

540

541 **DATA AVAILABILITY**

542 The Cre^{Cat} (residues 127- 343) backbone chemical shift assignments have been deposited
543 in the Biological Magnetic Resonance Data Bank, www.bmrb.wisc.edu (accession no. 50270).

544

545 **ACKNOWLEDGEMENTS**

546 We thank Dr. Chunhua Yuan, Dr. Alex Hansen and Dr. Arpad Somogyi of the Ohio State
547 University Campus Chemical Instrumentation Center for assistance with NMR experimental setup
548 and mass spectrometry analysis and Dr. Eric Danhart for guidance with NMR data processing.
549 We also thank Dr. Gregory Van Duyne (U. Penn) for providing the plasmids encoding Cre. This
550 study was supported by NIH grant R01 GM122432 (to M.P.F), NSF MCB grant 0092962 (to
551 M.P.F), and NIH/NIGMS grant 1P41GM111135 (to NMRBox).

552

553 **AUTHOR CONTRIBUTIONS**

554 Author contributions: A.U., C.A. and D.K.Y. and M.P.F. designed experiments; A.U., C.A.,
555 D.K.Y and D.P. performed research; A.U., D.K.Y., C.A., K.S. and M.P.F. analyzed and
556 interpreted data; and A.U. and M.P.F. wrote the manuscript.

557

558 **COMPETING INTERESTS**

559 The authors declare no competing financial interests.

560

561 **REFERENCES**

562 1. Bucholtz, F. Principles of site-specific recombinase (SSR) technology. *J. Vis. Exp.*
563 (2008) doi:10.3791/718.

564 2. Nunes-Düby, S. E., Kwon, H. J., Tirumalai, R. S., Ellenberger, T. & Landy, A.
565 Similarities and differences among 105 members of the Int family of site-specific
566 recombinases. *Nucleic Acids Res.* **26**, 391–406 (1998).

567 3. Wirth, D. *et al.* Road to precision: recombinase-based targeting technologies for
568 genome engineering. *Current Opinion in Biotechnology* (2007)
569 doi:10.1016/j.copbio.2007.07.013.

570 4. Fogg, P. C. M., Colloms, S., Rosser, S., Stark, M. & Smith, M. C. M. New applications
571 for phage integrases. *Journal of Molecular Biology* (2014)
572 doi:10.1016/j.jmb.2014.05.014.

573 5. Van Duyne, G. D. Cre Rcombinase. *Microbiol. Spectr.* (2015).

574 6. Meinke, G., Bohm, A., Hauber, J., Pisabarro, M. T. & Buchholz, F. Cre Recombinase
575 and Other Tyrosine Recombinases. *Chem. Rev.* (2016)
576 doi:10.1021/acs.chemrev.6b00077.

577 7. Lanza, A. M., Dyess, T. J. & Alper, H. S. Using the Cre/lox system for targeted
578 integration into the human genome: LoxFAS-loxP pairing and delayed introduction of
579 Cre DNA improve gene swapping efficiency. *Biotechnol. J.* (2012)
580 doi:10.1002/biot.201200034.

581 8. Grindley, N. D. F., Whiteson, K. L. & Rice, P. A. Mechanisms of Site-Specific
582 Recombination. *Annu. Rev. Biochem.* (2006)
583 doi:10.1146/annurev.biochem.73.011303.073908.

584 9. Landy, A. The λ Integrase Site-specific Recombination Pathway. *Microbiol. Spectr.*
585 (2015) doi:10.1128/microbiolspec.mdna3-0051-2014.

586 10. Gaj, T., Gersbach, C. A. & Barbas, C. F. ZFN, TALEN, and CRISPR/Cas-based
587 methods for genome engineering. *Trends in Biotechnology* (2013)
588 doi:10.1016/j.tibtech.2013.04.004.

589 11. Cox, D. B. T., Platt, R. J. & Zhang, F. Therapeutic genome editing: Prospects and
590 challenges. *Nature Medicine* (2015) doi:10.1038/nm.3793.

591 12. Groth, A. C. & Calos, M. P. Phage integrases: Biology and applications. *Journal of*
592 *Molecular Biology* (2004) doi:10.1016/j.jmb.2003.09.082.

593 13. Craig, N. L. Conservative site-specific recombination. 77–105 (1988).

594 14. Birling, M. C., Goffflot, F. & Warot, X. Site-specific recombinases for manipulation of the
595 mouse genome. *Methods Mol. Biol.* (2009) doi:10.1007/978-1-60327-019-9_16.

596 15. Sternberg, N. Bacteriophage P1 site-specific recombination. *J. Mol. Biol.* **150**, 603–608
597 (1981).

598 16. Guo, F., Gopaul, D. N. & Van Duyne, G. D. Structure of Cre recombinase complexed
599 with DNA in a site-specific recombination synapse. *Nature* (1997) doi:10.1038/37925.

600 17. Ghosh, K., Guo, F. & Van Duyne, G. D. Synapsis of loxP sites by cre recombinase. *J.*
601 *Biol. Chem.* (2007) doi:10.1074/jbc.M703283200.

602 18. Ghosh, K. & Van Duyne, G. D. Cre-loxp biochemistry. *Methods* (2002)
603 doi:10.1016/S1046-2023(02)00244-X.

604 19. Gopaul, D. N., Guo, F. & Van Duyne, G. D. Structure of the Holliday junction
605 intermediate in Cre-loxP site-specific recombination. *EMBO J.* **17**, 4175–4187 (1998).

606 20. Martin, S. S., Pulido, E., Chu, V. C., Lechner, T. S. & Baldwin, E. P. The order of strand
607 exchanges in Cre-LoxP recombination and its basis suggested by the crystal structure
608 of a Cre-LoxP holliday junction complex. *J. Mol. Biol.* (2002) doi:10.1016/S0022-
609 2836(02)00246-2.

610 21. Ghosh, K., Lau, C. K., Gupta, K. & Van Duyne, G. D. Preferential Synapsis of Loxp
611 Sites Drives Ordered Strand Exchange in Cre-Loxp Site-Specific Recombination. *Nat.*
612 *Chem. Biol.* (2005) doi:10.1038/nchembio733.

613 22. Van Duyne, G. D. A structural view of Cre-loxP site-specific recombination. *Annual*
614 *Review of Biophysics and Biomolecular Structure* (2001)
615 doi:10.1146/annurev.biophys.30.1.87.

616 23. Rajeev, L., Malanowska, K. & Gardner, J. F. Challenging a Paradigm: the Role of DNA
617 Homology in Tyrosine Recombinase Reactions. *Microbiol. Mol. Biol. Rev.* (2009)
618 doi:10.1128/mmbr.00038-08.

619 24. Seah, N. E. *et al.* Nucleoprotein architectures regulating the directionality of viral
620 integration and excision. *Proc. Natl. Acad. Sci. U. S. A.* (2014)
621 doi:10.1073/pnas.1413019111.

622 25. Baldwin, E. P. *et al.* A specificity switch in selected Cre recombinase variants is
623 mediated by macromolecular plasticity and water. *Chem. Biol.* (2003)
624 doi:10.1016/j.chembiol.2003.10.015.

625 26. Duyne, G. D. Van. A STRUCTURAL VIEW OF Cre-loxP SITE -SPECIFIC
626 RECOMBINATION. *Annu. Rev. Biophys. Biomol. Struct.* (2001).

627 27. Zhang, C. *et al.* Redesign of the monomer-monomer interface of Cre recombinase
628 yields an obligate heterotetrameric complex. *Nucleic Acids Res.* (2015)
629 doi:10.1093/nar/gkv901.

630 28. Aihara, H., Kwon, H. J., Nunes-Düby, S. E., Landy, A. & Ellenberger, T. A
631 conformational switch controls the DNA cleavage activity of λ integrase. *Mol. Cell*
632 (2003) doi:10.1016/S1097-2765(03)00268-5.

633 29. Subramaniam, S., Tewari, A. K., Nunes-Duby, S. E. & Foster, M. P. Dynamics and
634 DNA substrate recognition by the catalytic domain of lambda integrase. *J. Mol. Biol.*
635 **329**, 423–439 (2003).

636 30. Serre, M. C. *et al.* The Carboxy-Terminal αN Helix of the Archaeal XerA Tyrosine
637 Recombinase Is a Molecular Switch to Control Site-Specific Recombination. *PLoS One*
638 (2013) doi:10.1371/journal.pone.0063010.

639 31. Hickman, A. B., Waninger, S., Scocca, J. J. & Dyda, F. Molecular organization in site-
640 specific recombination: The catalytic domain of bacteriophage HP1 integrase at 2.7 Å
641 resolution. *Cell* (1997) doi:10.1016/S0092-8674(00)80202-0.

642 32. Kazmierczak, R. A., Swalla, B. M., Burgin, A. B., Gumport, R. I. & Gardner, J. E.
643 Regulation of site-specific recombination by the C-terminus of λ integrase. *Nucleic*
644 *Acids Res.* **30**, 5193–5204 (2002).

645 33. Gibb, B. *et al.* Requirements for catalysis in the Cre recombinase active site. *Nucleic*
646 *Acids Res.* **38**, 5817–5832 (2010).

647 34. Hoess, R., Abremski, K., Irwin, S., Kendall, M. & Mack, A. DNA specificity of the cre
648 recombinase resides in the 25 kDa carboxyl domain of the protein. *J. Mol. Biol.* **216**,
649 873–882 (1990).

650 35. Rufer, A. W. Non-contact positions impose site selectivity on Cre recombinase. *Nucleic*
651 *Acids Res.* **30**, 2764–2771 (2002).

652 36. Kim, S. T., Kim, G. W., Lee, Y. S. & Park, J. S. Characterization of Cre-loxP interaction
653 in the major groove: Hint for structural distortion of mutant Cre and possible strategy

654 for HIV-1 therapy. *J. Cell. Biochem.* **80**, 321–327 (2000).

655 37. Lee, L. & Sadowski, P. D. Identification of Cre residues involved in synapsis,
656 isomerization, and catalysis. *J. Biol. Chem.* **278**, 36905–36915 (2003).

657 38. Kay, L. E., Torchia, D. A. & Bax, A. Backbone Dynamics of Proteins As Studied by 15N
658 Inverse Detected Heteronuclear NMR Spectroscopy: Application to Staphylococcal
659 Nuclease. *Biochemistry* (1989) doi:10.1021/bi00449a003.

660 39. Yuan, P. Structural and biochemical studies of site-specific recombinases. *Diss.*
661 *available from ProQuest* 1–182 (2008).

662 40. Foster, M. P. *et al.* Chemical shift as a probe of molecular interfaces: NMR studies of
663 DNA binding by the three amino-terminal zinc finger domains from transcription factor
664 IIIA. *J. Biomol. NMR* (1998) doi:10.1023/A:1008290631575.

665 41. Williamson, M. P. Using chemical shift perturbation to characterise ligand binding.
666 *Progress in Nuclear Magnetic Resonance Spectroscopy* (2013)
667 doi:10.1016/j.pnmrs.2013.02.001.

668 42. Battiste, J. L. & Wagner, G. Utilization of site-directed spin labeling and high-resolution
669 heteronuclear nuclear magnetic resonance for global fold determination of large
670 proteins with limited nuclear overhauser effect data. *Biochemistry* (2000)
671 doi:10.1021/bi000060h.

672 43. Marius Clore, G. & Iwahara, J. Theory, practice, and applications of paramagnetic
673 relaxation enhancement for the characterization of transient low-population states of
674 biological macromolecules and their complexes. *Chem. Rev.* (2009)
675 doi:10.1021/cr900033p.

676 44. Clore, G. M. Practical Aspects of Paramagnetic Relaxation Enhancement in Biological
677 Macromolecules. in *Methods in Enzymology* (2015). doi:10.1016/bs.mie.2015.06.032.

678 45. Altenbach, C., Oh, K. J., Trabanino, R. J., Hideg, K. & Hubbell, W. L. Estimation of
679 inter-residue distances in spin labeled proteins at physiological temperatures:
680 Experimental strategies and practical limitations. *Biochemistry* (2001)
681 doi:10.1021/bi011544w.

682 46. DeLano, W. L. Pymol: An open-source molecular graphics tool. *CCP4 Newsl. Protein*

683 *Crystallogr.* (2002).

684 47. Gruene, T. *et al.* Integrated analysis of the conformation of a protein-linked spin label
685 by crystallography, EPR and NMR spectroscopy. *J. Biomol. NMR* (2011)
686 doi:10.1007/s10858-011-9471-y.

687 48. Janowska, M. K. & Baum, J. Intermolecular paramagnetic relaxation enhancement
688 (PRE) studies of transient complexes in intrinsically disordered proteins. in *Methods in*
689 *Molecular Biology* (2015). doi:10.1007/978-1-4939-2978-8_3.

690 49. Brault, V., Besson, V., Magnol, L., Duchon, A. & Hérault, Y. Cre/loxP-mediated
691 chromosome engineering of the mouse genome. *Handbook of Experimental*
692 *Pharmacology* (2007) doi:10.1007/978-3-540-35109-2-2.

693 50. Sengupta, R. *et al.* Viral Cre-LoxP tools aid genome engineering in mammalian cells.
694 *J. Biol. Eng.* (2017) doi:10.1186/s13036-017-0087-y.

695 51. Esposito, D. & Scocca, J. J. The integrase family of tyrosine recombinases: Evolution
696 of a conserved active site domain. *Nucleic Acids Res.* (1997)
697 doi:10.1093/nar/25.18.3605.

698 52. Clore, G. M. Seeing the invisible by paramagnetic and diamagnetic NMR. *Biochem.*
699 *Soc. Trans.* (2013) doi:10.1042/BST20130232.

700 53. Yoshizawa, S., Kawai, G., Watanabe, K., Miura, K. I. & Hirao, I. GNA trinucleotide loop
701 sequences producing extraordinarily stable DNA minihairpins. *Biochemistry* (1997)
702 doi:10.1021/bi961738p.

703 54. Delaglio, F. *et al.* NMRPipe: A multidimensional spectral processing system based on
704 UNIX pipes. *J. Biomol. NMR* (1995) doi:10.1007/BF00197809.

705 55. Norris, M., Fetler, B., Marchant, J. & Johnson, B. A. NMRFx Processor: a cross-
706 platform NMR data processing program. *J. Biomol. NMR* (2016) doi:10.1007/s10858-
707 016-0049-6.

708 56. Johnson, B. A. Using NMRView to visualize and analyze the NMR spectra of
709 macromolecules. *Methods Mol. Biol.* (2004) doi:10.1385/1-59259-809-9:313.

710 57. Bahrami, A., Assadi, A. H., Markley, J. L. & Eghbalnia, H. R. Probabilistic interaction
711 network of evidence algorithm and its application to complete labeling of peak lists from

712 protein NMR spectroscopy. *PLoS Comput. Biol.* (2009)
713 doi:10.1371/journal.pcbi.1000307.

714 58. Keller, R. *The computer aided resonance assignment tutorial*. *Goldau, Switzerland:*
715 *Cantina Verlag* (2004).

716 59. Sjodt, M. & Clubb, R. Nitroxide Labeling of Proteins and the Determination of
717 Paramagnetic Relaxation Derived Distance Restraints for NMR Studies. *BIO-*
718 *PROTOCOL* (2017) doi:10.21769/bioprotoc.2207.

719 60. Iwahara, J., Schwieters, C. D. & Clore, G. M. Ensemble Approach for NMR Structure
720 Refinement against 1H Paramagnetic Relaxation Enhancement Data Arising from a
721 Flexible Paramagnetic Group Attached to a Macromolecule. *J. Am. Chem. Soc.* (2004)
722 doi:10.1021/ja031580d.

723 61. Conway, P., Tyka, M. D., DiMaio, F., Konerding, D. E. & Baker, D. Relaxation of
724 backbone bond geometry improves protein energy landscape modeling. *Protein Sci.*
725 (2014) doi:10.1002/pro.2389.

726 62. Khatib, F. *et al.* Algorithm discovery by protein folding game players. *Proc. Natl. Acad.*
727 *Sci. U. S. A.* (2011) doi:10.1073/pnas.1115898108.

728 63. Nivón, L. G., Moretti, R. & Baker, D. A Pareto-Optimal Refinement Method for Protein
729 Design Scaffolds. *PLoS One* (2013) doi:10.1371/journal.pone.0059004.

730 64. Tyka, M. D. *et al.* Alternate states of proteins revealed by detailed energy landscape
731 mapping. *J. Mol. Biol.* (2011) doi:10.1016/j.jmb.2010.11.008.

732 65. Leaver-Fay, A. *et al.* Rosetta3: An object-oriented software suite for the simulation and
733 design of macromolecules. in *Methods in Enzymology* (2011). doi:10.1016/B978-0-12-
734 381270-4.00019-6.

735 66. Park, H. *et al.* Simultaneous Optimization of Biomolecular Energy Functions on
736 Features from Small Molecules and Macromolecules. *J. Chem. Theory Comput.* (2016)
737 doi:10.1021/acs.jctc.6b00819.

738

739 **FIGURES**

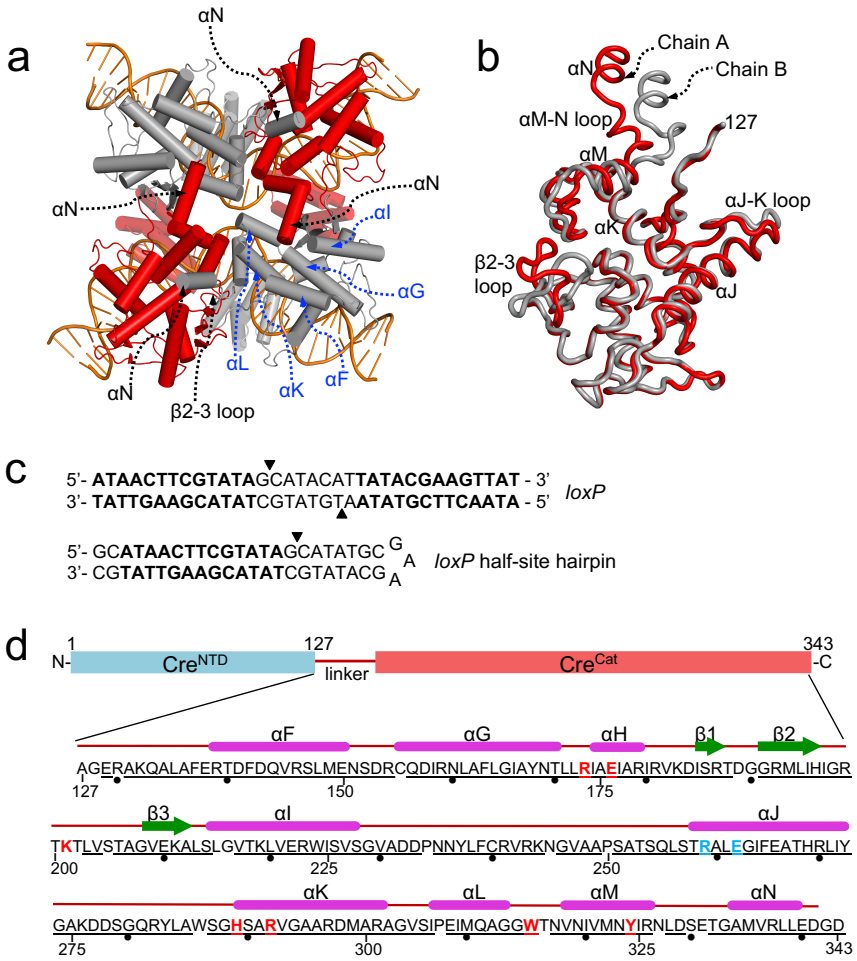

740

741

742 **Fig. 1** Conformational changes underlie coordinated DNA recombination by Cre
743 recombinase.

744 **a** Tetrameric synaptic complex of four Cre protomers bound to two *loxP* DNA duplexes (PDB
745 ID 2HOI), viewed from the catalytic domain, Cre^{Cat}. C-terminal helix αN of each protomer
746 packs into a *trans* surface cavity (labeled in blue) in the adjacent protomer.

747 **b** Superposition of Cre^{Cat} domains from "inactive" (red) and "active" (gray) Cre protomers
748 (PDB ID 2HOI: chains A and B, respectively) highlight differences in the β2-3 loop, helix αM,
749 αM-N loop and C-terminal helix αN.

750 **c** *loxP* DNA, and the *loxP* half-site hairpin DNA sequence used in these studies; arrows
751 indicate cleavage sites in full-length *loxP* DNA.

752 **d** Domain map of Cre recombinase. Residues 1-126 (blue) comprise the N-terminal domain
753 (Cre^{NTD}). The interdomain linker and C-terminal catalytic domain comprise the Cre^{Cat}
754 construct (residues 127- 343) used in these studies (pink). Sequence of the Cre^{Cat} construct
755 is shown (numbered 127 to 343; dots shown as guide) with corresponding secondary
756 structure elements from synaptic complex crystal structure (PDB ID 2HOI, chain B); residues
757 G342 and D343 are not modeled in electron density maps. Active site and DNA binding
758 specificity determinant residues are highlighted in red and cyan respectively. Backbone
759 amide NMR chemical shift resonance assignments were made for all underlined residues.
760

761

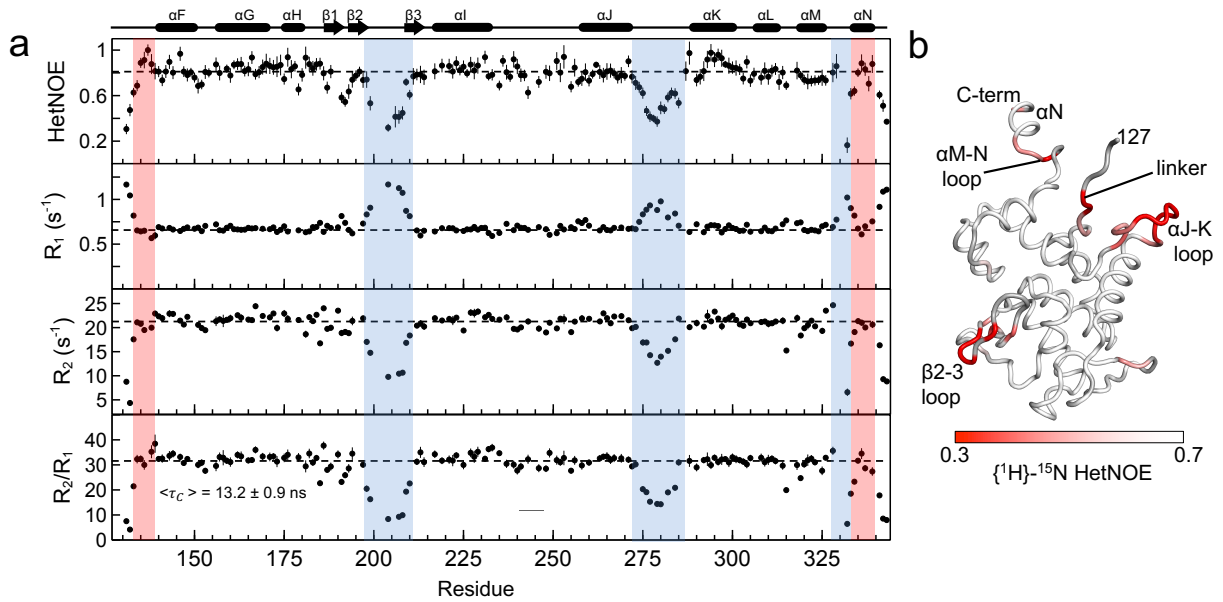

762

763 **Fig 2.** Cre^{Cat} loops β2-3, αJ-K and αM-N, but not helix αN, exhibit fast timescale dynamics.

764 **a** $\{^1H\}$-^{15}N Heteronuclear NOE, ^{15}N longitudinal R_1 relaxation rate constant (s^{-1}), ^{15}N
765 transverse R_2 relaxation rate constant (s^{-1}) and corresponding R_2/R_1 ratios for Cre^{Cat}; 800
766 MHz; 298 K. Dashed lines in panels represent average values calculated excluding regions
767 of fast timescale dynamics. The secondary structure elements of Cre^{Cat} synaptic complex
768 crystal structure (PDB ID 2HOI, chain B) are shown above the plot for comparison.

b {^{1}H}-^{15}N HetNOE values for Cre^{Cat} mapped onto the crystal structure (PDB ID 2HOI, chain B) as a linear gradient from red (= 0.3) to white (≥ 0.7). Residues with no data are shown in gray.

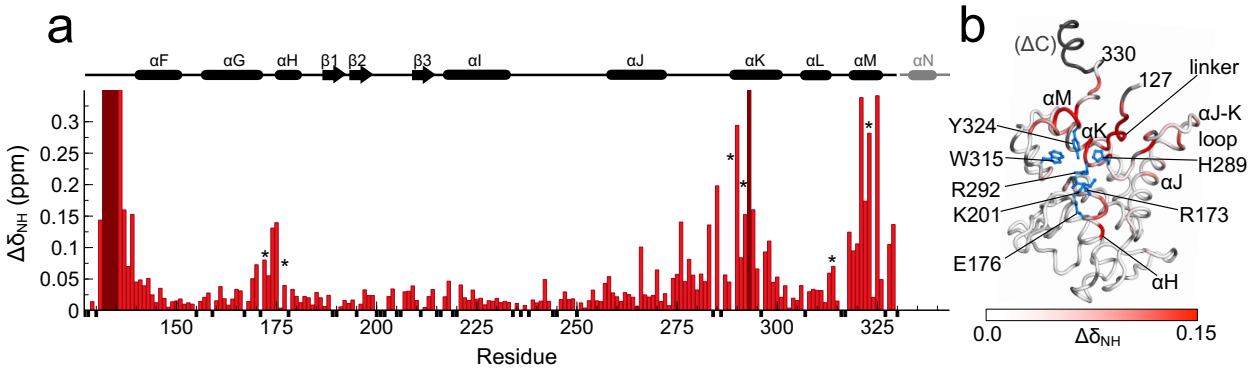

Fig. 3 C-terminal deletion results in CSPs in the core of Cre^{Cat}.

a Per-residue amide CSPs [$\Delta\delta_{NH} = (\Delta\delta_H^2 + \Delta\delta_N^2/25)^{1/2}$] of Cre^{Cat} upon truncation of last 13 amino acid from the C terminus Δ(E331- D343) (red bars). The secondary structure elements of Cre synaptic complex crystal structure (PDB ID 2HOI, chain B) are shown above the plot. Asterisks indicate regions of high CSP containing active site residues R173, E176, H289, R292, W315 and Y324. Residues that showed largest CSPs or peak broadening beyond detection (assigned in Cre^{Cat} but unassigned in Cre^{Cat}ΔC spectrum) are shown in maroon. Unassigned residues are indicated by small negative black bars.

b Amide CSPs mapped onto the crystal structure (PDB ID 2HOI, chain B) as a linear gradient from white (= 0.0 ppm) to red (≥ 0.15 ppm). Sidechains of active site residues R173, E176, K201 (modeled using PyMOL), H289, R292, W315 and Y324 are shown in blue. Truncated C-terminal residues Δ(E331- D343) and unassigned residues are indicated in gray.

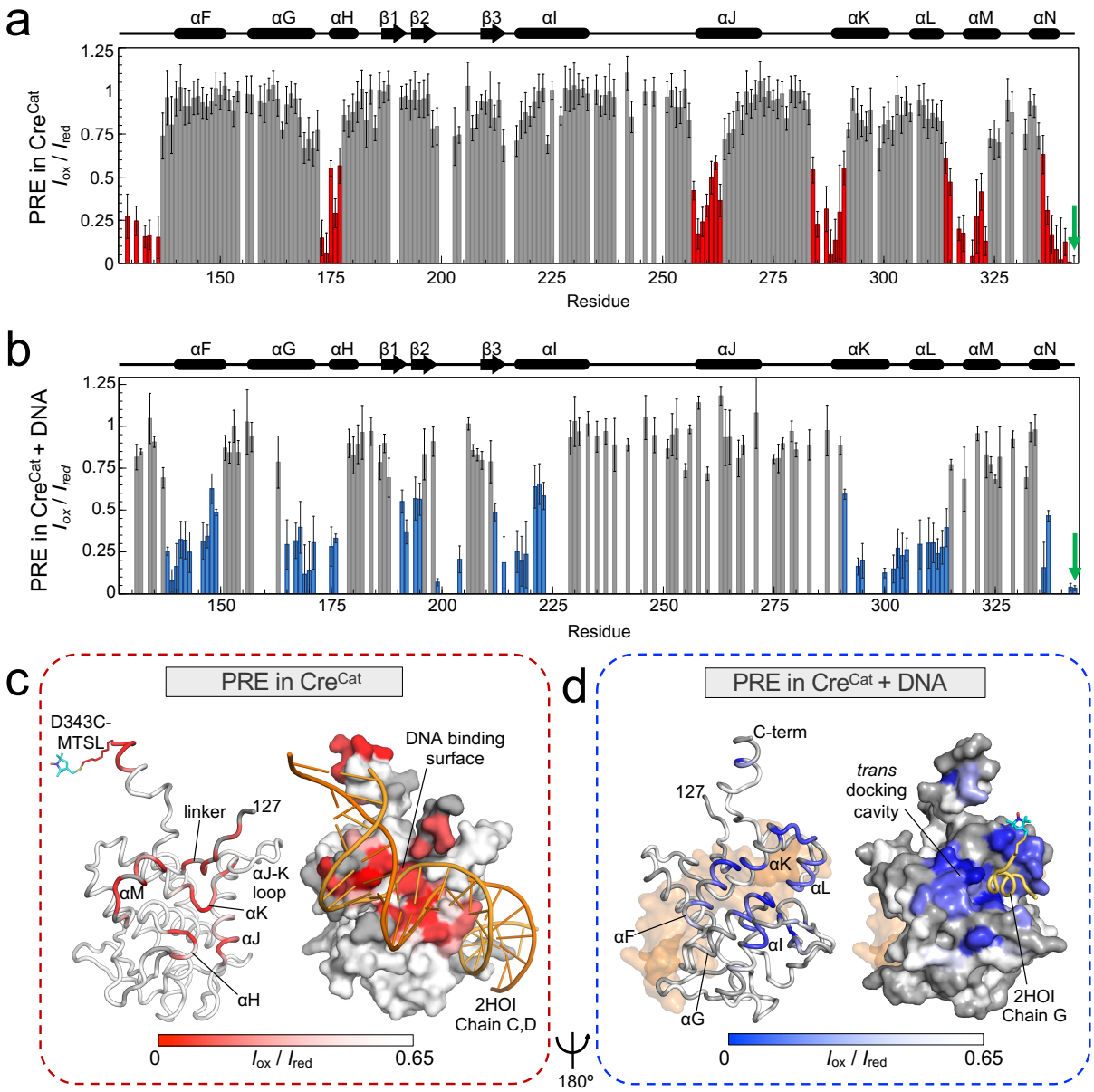

Fig. 4 PRE-NMR data reveal a *cis* to *trans* docking conformational switch in the Cre^{Cat} C-terminus upon DNA binding.

a Per-residue amide PRE-NMR normalized intensity ratios (I_{ox}/I_{red}) of free Cre^{Cat} C155A/C240A/D343C generated using an MTSL paramagnetic probe at C-terminal residue C343 (green arrow); strong PRE effects ($I_{ox}/I_{red} < 0.65$) are shown in red. Secondary structure elements of Cre synaptic complex crystal structure (PDB ID 2HOI, chain B) are shown. Uncertainties are propagated from the signal-to-noise ratio of individual resonances.

797 **b** Per-residue amide PRE-NMR normalized intensity ratios (I_{ox}/I_{red}) for Cre^{Cat}
798 C155A/C240A/D343C bound to *loxP* half-site DNA generated using MTSL paramagnetic
799 probe at C-terminal residue C343 (green arrow); strong PRE effects ($I_{ox}/I_{red} < 0.65$) are shown
800 in blue. Uncertainties are propagated from the signal-to-noise ratio of individual resonances.

801 **c** I_{ox}/I_{red} PRE values from free Cre^{Cat} mapped to the structure of a protomer in the crystal
802 structure (PDB ID 2HOI, chain B; G342, C343-MTSL modeled) as a gradient from red (I_{ox}/I_{red}=
803 0) to white (I_{ox}/I_{red}= 0.65). Residues with no PRE data are shown in gray. Juxtaposed
804 equivalent surface representation (same orientation) along with a portion of the *loxP* DNA, as
805 seen in the crystal (PDB ID 2HOI, chains C and D) is shown in orange to illustrate the PRE
806 effects mapping to the DNA binding surface.

807 **d** I_{ox}/I_{red} PRE values from the Cre^{Cat}-DNA complex mapped to the structure of a protomer in
808 the crystal structure (PDB ID 2HOI, chain B; G342, C343 modeled) as a gradient from blue
809 (I_{ox}/I_{red}= 0) to white (I_{ox}/I_{red}= 0.65). Bound DNA (PDB ID 2HOI, chains C and D) is shown in
810 pale orange. Residues with no PRE data are shown in gray. Juxtaposed equivalent surface
811 representation (same orientation) along with C-terminal helix αN region from an adjacent
812 MTSL-tagged protomer (PDB ID 2HOI, chain G: E331-D341 and G342, C343-MTSL
813 modeled) is shown in yellow to illustrate the PRE effects mapping to protein-protein *trans*
814 docking surface cavity. Orientation of Cre^{Cat} is rotated approximately 180° between Fig. 4**c**
815 and **d.**

816

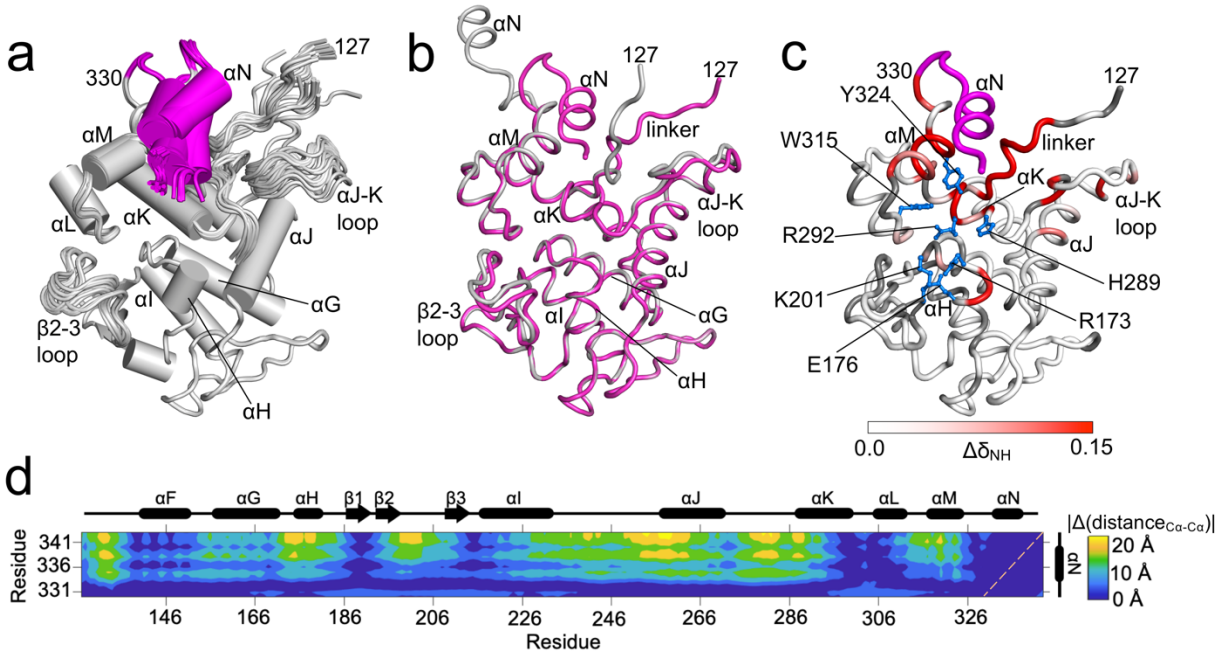

Fig. 5 PRE-derived ensemble models of free Cre^{Cat} shows *cis* docking of C-terminus over the Cre^{Cat} active site.

a Top fifty PRE-derived ROSETTA models of free Cre^{Cat} showing *cis* docking of C-terminal region (E331- D343; in magenta).

b Overlay of lowest ROSETTA energy member of the PRE-derived ensemble model (magenta) and the crystal structure protomer (PDB ID 2HOI, chain A) (gray).

c CSPs in free Cre^{Cat} upon C-terminal truncation Δ(E331- D343) (magenta) mapped onto the lowest energy member of the PRE-derived ensemble model as a linear gradient from white (0.0 ppm) to red (≥ 0.15 ppm). Unassigned residues are shown in gray (as in Fig. 3**b**).

d Difference in the inter-residue Cα-Cα contact map between the top ten PRE-derived models and the DNA bound tetrameric crystal structure (PDB ID 2HOI, chain A) (absolute values of changes in inter-residue distances $|\Delta distance_{C\alpha\text{-}C\alpha}|$ (Å) are shown by a three-color heatmap from blue to yellow). The secondary structure elements of Cre synaptic complex crystal structure (PDB ID 2HOI, chain B) are shown along the axes. Diagonal is shown as dashed line (orange).

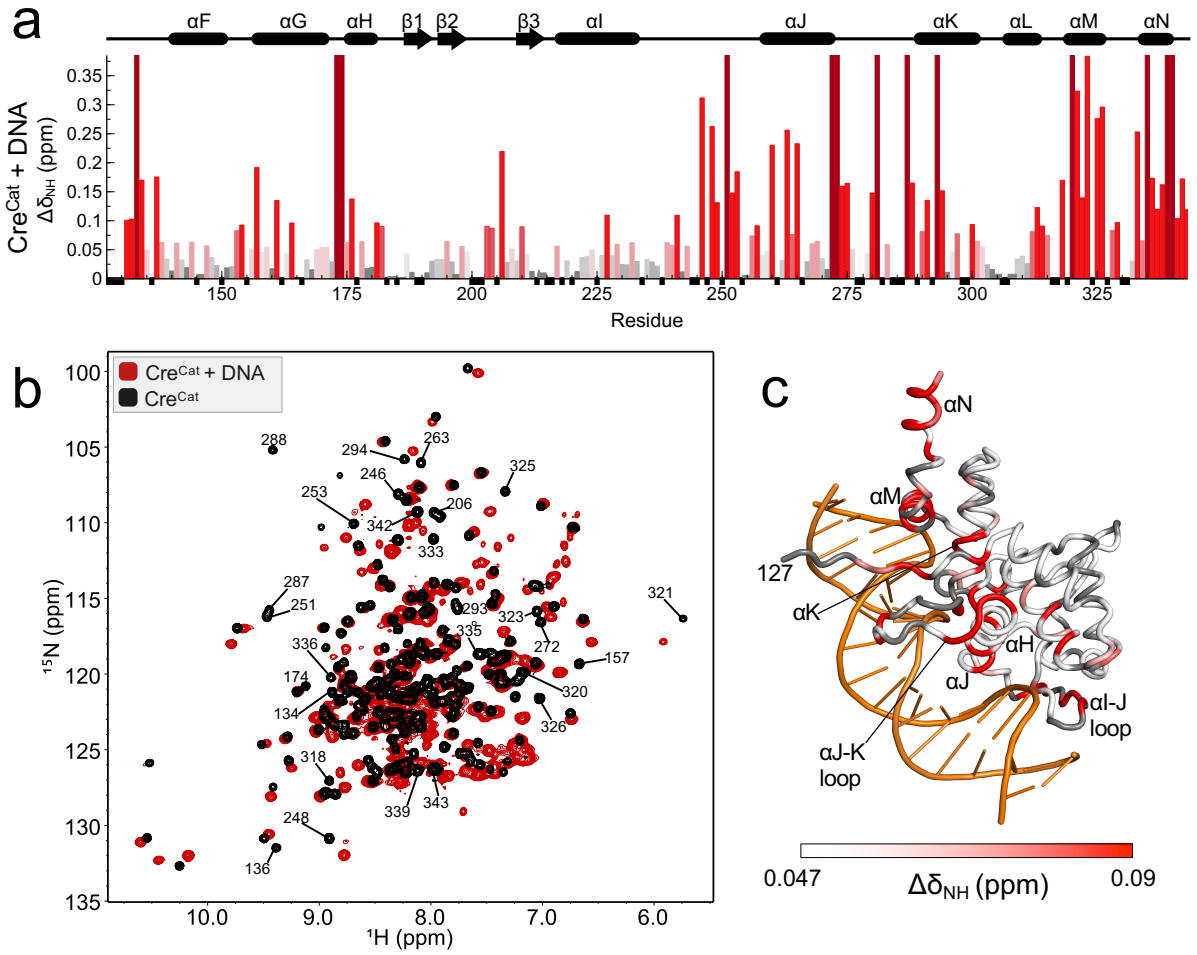

834

835 **Fig. 6**. C-terminal helix αN region of Cre^{Cat} is perturbed upon binding to *loxP* DNA

836 **a** Per-residue amide CSPs [$\Delta\delta_{NH} = (\Delta\delta_H^2 + \Delta\delta_N^2/25)^{1/2}$] of Cre^{Cat} upon binding to *loxP* half-
837 site hairpin DNA with a linear color ramp from gray (= 0 ppm) to red (≥ twice the Δδ SD (0.047
838 ppm)). Largest CSPs, or those that resulted in peak-broadening beyond detectability
839 (assigned in free Cre^{Cat} but unassigned in the Cre^{Cat}- DNA complex) are shown in maroon.
840 Unassigned residues are indicated by small negative black bars. Secondary structure
841 elements of Cre synaptic complex crystal structure (PDB ID 2HOI, chain B) are shown above
842 the plot.

843 **b** Overlay of ^1H-^{15}N TROSY-HSQC spectra of free Cre^{Cat} (black) and bound to a DNA half-
844 site (red) with select residue assignments indicated (> 3 SD ppm).

845 **c** CSPs mapped onto the crystal structure (PDB ID 2HOI, chain B) as a linear gradient from
846 white (≤ 1 SD ppm) to red (≥ 2 SD ppm). Unassigned residues are shown in gray.
847